Electron-impact detachment from PO_n^- ($n=0-3$)

Annette Svendsen, Lutz Lammich, Marianne Sanggaard, and Lars H. Andersen
Department of Physics and Astronomy, University of Aarhus, DK-8000 Aarhus C, Denmark
(Received 22 June 2007; published 12 September 2007)

Electron detachment from PO_n^- ($n=0-3$) by electron impact was studied for incident-electron energies in the range from 0 to 50 eV. In all cases, the cross section for electron detachment exhibits a well-defined onset at a threshold energy that is significantly higher than the electron binding energy. For P^-, PO^-, and PO_2^-, the overall shape of the detachment cross section is represented fairly well by a classical model cross section. For PO_3^-, however, deviations occur. It is suggested that deviations appear because the detachment process is dependent on the relative orientation of the molecular ion with respect to the incoming electron. For all the molecular ions studied here, the dominant reaction channel is pure detachment without fragmentation of the molecule. At higher energies, electron impact furthermore results in dissociative detachment where a P–O bond is broken. Three- and four-body fragmentation is found to be negligible.

DOI: 10.1103/PhysRevA.76.032707 PACS number(s): 34.80.Kw

I. INTRODUCTION

The first experimental study of electron-impact detachment from negative ions was reported already in 1966 by Tisone and Branscomb [1] who studied the detachment process

$$H^- + e^- \rightarrow H + 2e^-. \qquad (1)$$

This process was considered to be an important mechanism leading to the destruction of H^- in the atmosphere of the Sun where H^- is the predominant source of the opacity [2–4]. Knowledge about the absolute detachment cross section and its energy dependence was therefore crucial for the modeling of stellar photospheres, and this fact initially triggered the experimental investigations within the field. Throughout the 1970s, electron-impact detachment cross sections of several atomic anions were measured as a function of the electron kinetic energy (see Refs. [5–8] and references therein), but a common feature was lack of data in the cross section onset region. Only with the advent of magnetic storage rings and the use of merged beams in the 1990s did it become possible to investigate the cross-section behavior in the threshold region. Since then, several atomic anions have been studied [9–17] along with diatomic anions [18–24] and small polyatomic negative ions [25–30]. Moreover, the appearance of electrostatic storage rings [31] and ion traps [32,33] have made it possible to study electron detachment from large molecules like DNA building blocks [34,35] and other heavy, large molecular ions [36–38].

These studies have established that the detachment cross section is characterized by an effective threshold two to three times larger than the electron binding energy of target anion. This effect can be accounted for by the Coulomb repulsion in the incoming channel, which the projectile electron must overcome to cause detachment. Furthermore, the detachment cross section has a smooth energy dependence, which is expected due to the nonresonant character of the process. A comparison of the detachment cross sections for the various types of ions reveals that the cross section shapes are remarkably similar when scaled properly [20].

In need of a simple analytic expression that might be used to describe the near-threshold behavior of nonresonant detachment cross sections, a simple classical model was introduced by Andersen and co-workers [9]. This model assumes that detachment occurs with constant probability p if the projectile electron comes within a distance R_{th} of the anion. Assuming that the incoming electron experiences a purely repulsive Coulomb potential, an analytic expression for the distance of closest approach D_c can be found as a function of the impact parameter ρ and the energy E of the incoming electron. The nonresonant cross section is then modeled according to

$$\begin{aligned}\sigma_{\mathrm{NR}} &= 2\pi\int_0^\infty \rho\, d\rho \begin{cases} p & D_c(E,\rho) \le R_{\mathrm{th}} \\ 0 & D_c(E,\rho) > R_{\mathrm{th}} \end{cases} \\ &= p\pi R_{\mathrm{th}}^2 \max\left[0,\left(1-\frac{E_{\mathrm{th}}}{E}\right)\right], \qquad (2)\end{aligned}$$

where the classical threshold energy for detachment, $E_{\mathrm{th}} = 1/R_{\mathrm{th}}$ (in atomic units), has been introduced. This simple model has been successful in describing the near-threshold behavior of detachment cross sections for both atomic and molecular anions [9,10,20]. The model, however, assumes the target to be spherically symmetric, and consequently it might fail to reproduce the experimentally observed cross section behavior for highly asymmetric targets. In fact, signs of limitations have been observed in a few previous cases [37,39]. Here, we study electron-impact detachment from phosphorus oxide anions and further develop the classical model by taking into account the asymmetry of the target anion.

Another aspect of the electron-anion collision process is the possible formation and subsequent decay of a doubly charged anion, a dianion:

$$X^- + e^- \rightarrow X^{2-} \rightarrow \text{neutral products}. \qquad (3)$$

This process is a resonant process since the energy of the incoming electron must match that of the dianion for the reaction to occur. A resonant structure in the cross section for neutral fragment production therefore indicates the formation and subsequent decay of a dianion. Such resonance structures have been observed for some small polyatomic anions like, for example, C_2^- [18], CN^- [23], NO_2^- [25], and NO_3^- [27], but it remains a challenge to predict for which systems such states exist. To obtain more information about in which cases such resonance states might occur, we here compare results for PO_2^- and PO_3^- obtained in this work to previous results obtained for the electronic analogs of NO_2^- and NO_3^-.

II. EXPERIMENT

The technique used in the present experiments is described in detail elsewhere [20,27], and thus only a brief introduction is given here. The PO_n^- anions were formed in a Cs sputter ion source [40,41] with a cathode consisting of a mixture of 70% InP and 30% Ag. To produce the oxygen-containing anions, atmospheric air was furthermore let into the source, and the extracted ion currents were in the order of 10–100 nA. After mass selection and injection into the Aarhus STorage RIng Denmark (ASTRID) magnetic storage ring [42,43] at 150 keV, the circulating ions were accelerated by means of a radio-frequency system to final energies ranging from 1.72 MeV for PO_3^- to 4.41 MeV for P^-. The average pressure in the ring was $\sim 10^{-11}$ mbar which resulted in an average ion lifetime of several seconds. After having reached the final storage energy, the stored ion beam was merged with an essentially monoenergetic[1] beam of electrons provided by the electron-cooler device [44]. The beams were merged several seconds after extraction of the ions from the source, and the ions are therefore expected to be vibrationally cold during electron bombardment.

Neutral fragments created in collisions of the stored ions with electrons or residual gas are not affected by the dipole magnet following the electron-ion interaction region and thus leave the ring. Outside the ring, they hit an energy-sensitive surface-barrier solid-state detector (SSD) located behind the magnet. In order to extract the number of electron-induced events, the number of background events stemming from ions colliding with the residual gas must be subtracted from the total number of counts. This background subtraction is enabled by turning the electron beam on and off (chopped beam) at a frequency of 20 Hz.

The fragments emerging from a collision event all have essentially the same velocity, which is equal to the beam velocity, and accordingly each fragment carries a kinetic energy proportional to its mass. When impacting on the SSD, the fragments give rise to a signal dependent on their kinetic energy which is deposited in the detector. The SSD pulse-height spectrum therefore provides information on the fragment mass, and to illustrate this fact, an SSD spectrum from the PO_2^- experiment is shown in Fig. 1. In the spectrum, four peaks are evident corresponding to the detection of mass 16 (O), mass 31–32 (P, O_2, and O+O), mass 47 (PO and P+O), and mass 63 (any combination of one P and two O atoms).[2]

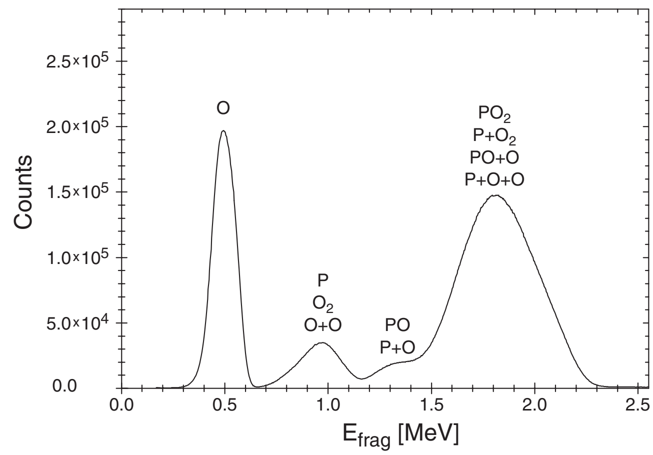

FIG. 1. Typical energy spectrum of neutral fragments recorded by the solid state detector with a PO_2^- beam of energy 1.9 MeV stored in the ring.

As also indicated in Fig. 1, a molecule cannot be distinguished from a group of molecular fragments of the same total mass arriving within a few microseconds since the two events deposit the same amount of energy. Furthermore, due to the finite energy resolution, one P atom cannot be distinguished from two O atoms as the total masses are very similar.

The electron-induced signal in each peak in the SSD spectrum was measured as a function of electron energy and converted into a cross section by normalizing the electron-induced count rate to the electron density and the number of ions in the interaction region. However, the absolute number of ions could not be obtained since the ion current was too low. Instead, the rate of background events stemming from residual gas collisions was used for normalization since this rate is proportional to the ion current. As a consequence, the obtained cross sections were not put on an absolute scale. The experimental data were corrected for toroid effects occurring in the electron cooler [12].

As described above, the solid-state detector measures the total energy deposited in the detector material during the stopping of the incoming fragments implying that, for example, two O atoms emerging from a collision event cannot be directly distinguished from an O_2 molecule. Nonetheless, this problem must be surpassed if the branching ratios between different reaction channels are to be found. The channels can be separated from each other by using a well-established grid technique [45–48] in which a mesh grid of finite transmission, T, is inserted in front of the detector. Now, channels leading to production of a neutral O_2 molecule contribute with probability T to the SSD peak corresponding to detection of mass 32. In contrast, channels producing two neutral O atoms contribute to the mass 32 SSD peak with probability T^2 and to the SSD peak corresponding to detection of mass 16 with probability $2T(1-T)$, as one of the O atoms might be stopped by the grid. With the insertion of a mesh grid, the relative intensities of the SSD peaks change dependent on the branching ratios, and hence it becomes possible to separate channels that would be indistinguishable without a grid.

[1] The energy spread is estimated to be 0.2 eV at collision energies in the range 10–20 eV.

[2] All masses are given in atomic mass units (amu).

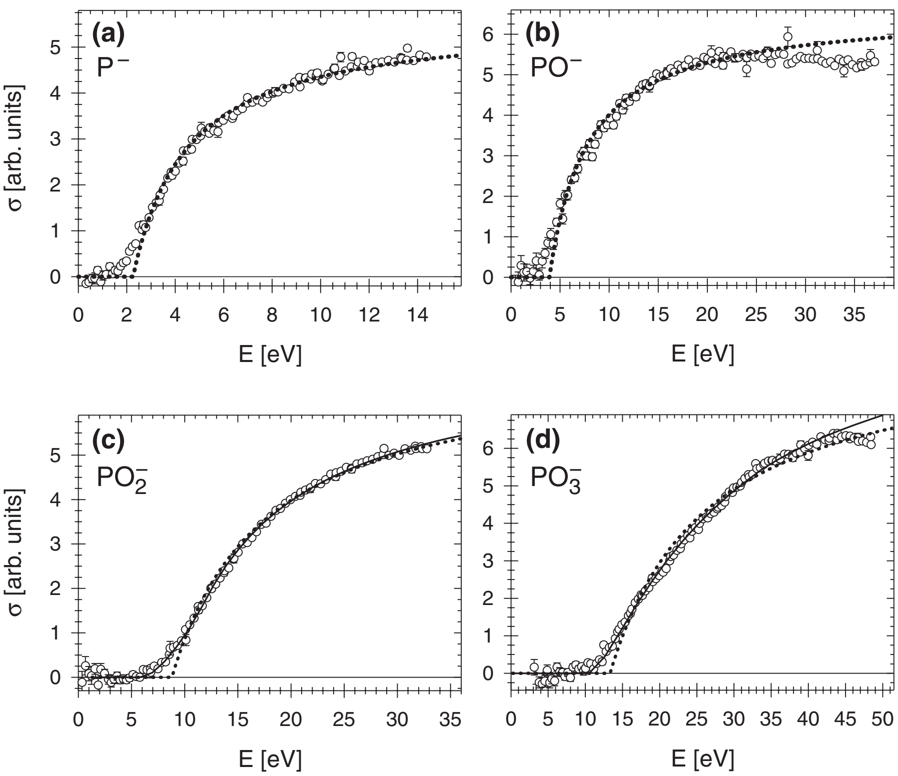

FIG. 2. Cross sections for electron-induced neutralization as a function of the collision energy for (a) P^-, (b) PO^-, (c) PO_2^-, and (d) PO_3^-. Open circles: experimental data; dotted curves: fits to the data by the spherical classical model [Eq. (2)]; solid curves: model cross sections for an elliptical reaction zone (see Sec. IV).

To extract the branching ratios, such grid measurements were performed for all molecular ions studied here with two grids of transmission 68% and 24% in addition to an equivalent measurement without a grid.

III. RESULTS

A. P^-

The detachment cross section for P^- is presented in Fig. 2(a). The cross section is seen to be zero below some onset energy at ~1.6 eV above which it increases smoothly with the collision energy. The dotted curve represents a fit by the classical model cross section [Eq. (2)]. The model provides a good description of the data, but small deviations are evident in the threshold region. The finite energy resolution of the experiment causes a smearing of the measured cross section, but since the energy spread is estimated to be ~0.2 eV, this effect alone cannot account for the discrepancy. Another effect that causes smearing in the threshold region is tunneling of the target electron out of the binding potential, an effect not included in the classical picture. The classical threshold energy for detachment extracted from the fit is 2.3 ± 0.1 eV.

B. PO^-

Figure 2(b) shows the cross section for neutralization of PO^-, which is the sum of the cross sections for pure detachment and dissociative detachment. The cross section for production of charged fragments is negligible in comparison and is therefore not shown. The neutralization cross section has an onset at ~3.0 eV and exhibits a smooth behavior as a function of the collision energy with a maximum at ~25 eV.

The dotted curve is a fit by the model cross section of Eq. (2). As seen, the agreement with the experimental data is good, but the decreasing tendency at high energies is not reproduced by the model. This decrease is due to the smaller momentum transfer in high energy collisions, and deviations occur since this effect is neglected by the classical model. The value for the classical threshold energy extracted from the fit is 3.9 ± 0.2 eV.

To investigate the relative importance of pure detachment and dissociative detachment, grid measurements were carried out at four energies between 0 and 30 eV. For PO^-, the following electron-induced reactions are relevant:

$$PO^- + e^- \to \begin{cases} PO + 2e^-, & \Delta E = 1.1\ \text{eV} \quad \text{(A)} \\ P + O + 2e^-, & \Delta E = 7.2\ \text{eV} \quad \text{(B)} \\ \left.\begin{array}{ll} P^- + O + e^-, & \Delta E = 6.5\ \text{eV} \\ P^+ + O + 3e^-, & \Delta E = 17.7\ \text{eV} \end{array}\right\} & \text{(C)} \\ \left.\begin{array}{ll} P + O^- + e^-, & \Delta E = 5.8\ \text{eV} \\ P + O^+ + 3e^-, & \Delta E = 20.9\ \text{eV} \end{array}\right\} & \text{(D)} \end{cases}, \tag{4}$$

where ΔE is the endothermic reaction energy. The reaction energies are calculated from the heats (or enthalpies) of formation as listed in the NIST Chemistry Webbook [49] which also includes references to the original measurements of the heats of formation. In the energy range where the branching ratio measurements were performed, no electron-induced signal was observed in the peaks corresponding to detection of single P or O atoms, implying that channels (C) and (D) do not contribute to the total cross section at these energies. The extracted branching ratios are shown in Fig. 3(a). As

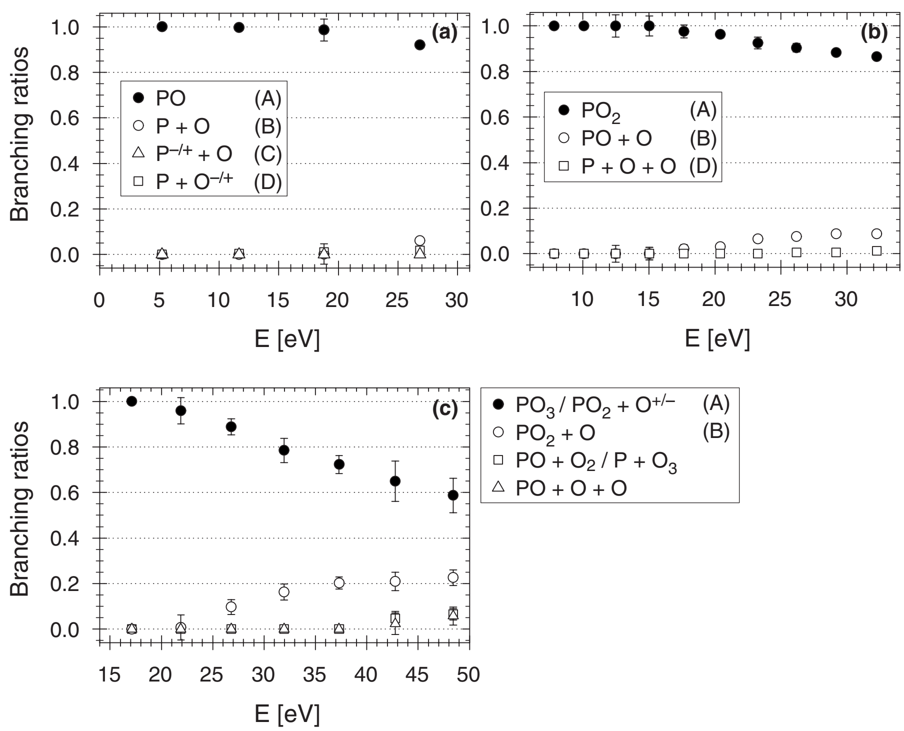

FIG. 3. Branching ratios for the different reaction channels observed after electron impact on (a) PO^-, (b) PO_2^-, and (c) PO_3^- as a function of the collision energy.

seen, the dominant reaction channel is pure detachment with a relative contribution of more than 91% at all four energies. Above 25 eV, this contribution apparently begins to decrease as dissociative detachment [channel (B)] is setting in. Note that even though this channel is more endothermic than channels (C) and (D), it contributes more to the electron-induced reactions in the studied energy range than the latter channels.

C. PO_2^-

The neutralization cross section for PO_2^- is seen in Fig. 2(c). It increases smoothly with the collision energy above an onset at ~6.5 eV. The cross section for production of charged particles is negligible in the investigated energy range and is therefore not shown.

A fit by the model cross section [Eq. (2)] is displayed as a dotted curve in the figure. The classical threshold energy for detachment of 8.8±0.2 eV is obtained by the fit. The fitted curve reproduces the data fairly well, but, again, the measured cross section exhibits a more smooth onset than predicted by the model cross section due to the neglect of tunneling in the model.

Branching ratio measurements were carried out at energies below 35 eV. The reaction channels contributing to the neutralization cross section here are

$$PO_2^- + e^- \rightarrow \begin{cases} PO_2 + 2e^-, & \Delta E = 3.6 \text{ eV} \quad (A) \\ PO + O + 2e^-, & \Delta E = 9.0 \text{ eV} \quad (B) \\ P + O_2 + 2e^-, & \Delta E = 10.0 \text{ eV} \quad (C) \\ P + 2O + 2e^-, & \Delta E = 15.1 \text{ eV} \quad (D) \end{cases} . \tag{5}$$

Again, the endothermic reaction energies, ΔE, are calculated from heats of formation listed in Ref. [49]. The results of the measurements are seen in Fig. 3(b). Below 17 eV, neutralization solely stems from pure detachment [channel (A)], whereas detachment plus dissociation into PO+O makes up an increasing fraction of all events at higher energies. At 32 eV, the two channels account for 86±2% and 8.8±1.0% of all events, respectively. All other channels constitute the remaining flux, each contributing less than 2%.

D. PO_3^-

For PO_3^-, it is not possible to separate neutralization events, that is production of PO_3 or neutral fragments of the same total mass, from events producing PO_2 (or neutral fragments of the same total mass). This is due to the limited energy resolution of the solid state detector used in this experiment to detect the low-energy heavy particles. The fragments lose energy on their way through the dead layer to the active area of the detector where they deposit their remaining energy. This energy loss is due to Coulomb interactions with nuclei and electrons of the detector material and scales with the square of the nuclear charge of the fragments, thus being more significant for heavier fragments [50]. Furthermore, the energy lost in the dead layer exhibits a broad distribution thereby causing a non-negligible spread in the detected energy deposit. The effect of the dead layer on the SSD spectrum is clearly seen in the spectrum shown in Fig. 4(a). The SSD peak corresponding to detection of mass 79 is not centered at the full beam energy of 1.72 MeV but is instead shifted to lower energies. More importantly, though, the two SSD peaks corresponding to detection of mass 79 and 63 are compressed into one single peak as the energy shifts are different for the two peaks and as the energy loss causes broadening of the peaks.

The cross section presented in Fig. 2(d) for PO_3^- is therefore the sum of the neutralization cross section and the cross

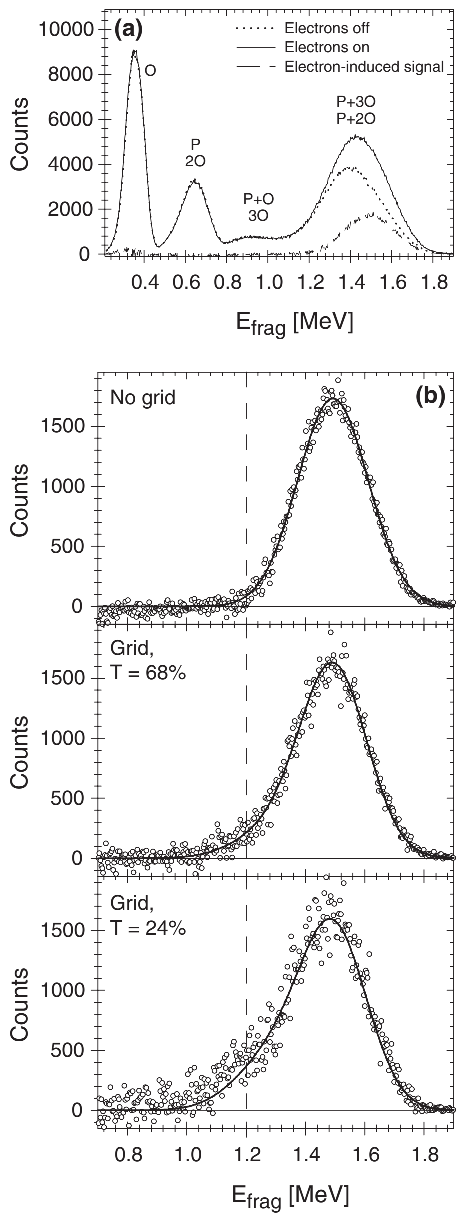

FIG. 4. (a) Energy spectrum of neutral fragments from a PO_3^- beam recorded by the solid state detector with and without the electron beam as well as the electron-induced signal. (b) Electron-induced signal for fragment energies in the range corresponding to masses 63 and 79 amu recorded with three different grid transmissions. The solid and dashed lines are to guide the eye.

section for production of one charged oxygen. At a collision energy of ~11.5 eV, the cross section has its onset, and it continues to rise up to ~45 eV. As for PO_2^-, the cross section for production of other charged fragments than only one oxygen is very small, and is therefore not shown.

The model cross section is found to give the best overall description of the data when using a threshold energy of 13.3±0.2 eV. However, the model provides a poor description of the data not only in the threshold region as expected, but rather in the entire energy range as the experimental cross section exhibits a markedly different overall shape than the model.

Measurements to identify the reaction channels in play were done at several energies in the range from 15 to 50 eV. It is found that the most important channels are

$$PO_3^- + e^- \rightarrow \begin{cases} \left.\begin{array}{ll} PO_3 + 2e^-, & \Delta E = 5.0 \text{ eV} \\ PO_2 + O^- + e^-, & \Delta E = 7.6 \text{ eV} \\ PO_2 + O^+ + 3e^-, & \Delta E = 22.7 \text{ eV} \end{array}\right\} & \text{(A)} \\ PO_2 + O + 2e^-, \quad \Delta E = 9.1 \text{ eV} & \text{(B)} \end{cases}, \tag{6}$$

where endothermic reaction energies again are calculated with the use of Ref. [49]. The three reactions listed as channel (A) are indistinguishable due to the limited energy resolution of the detector as explained above. It is obvious from Fig. 3(c) that channel (A) is the dominant channel in the entire energy range, but the relative contribution of this channel decreases, while channel (B) is setting in. At all energies in this range, the two channels constitute more than 80% of the electron-induced reactions.

Close inspection of the SSD pulse height spectra obtained using the different grids reveals indications that the main contribution to channel (A) might stem from pure detachment. A complete pulse height spectrum is shown in Fig. 4(a) together with the electron-induced signal in the energy range corresponding to detection of masses 79 and 63 amu for three different grids [Fig. 4(b)]. From the complete pulse height spectrum, it is clear that the electron-induced signal above 1.1 MeV peaks at higher energies than the corresponding residual-gas induced background signal which most likely contains contributions from both mass 63 and 79 amu. As some of the electron-induced events stem from channel (B), flux must be transferred from a neutral mass of 79 amu to mass 63 amu upon insertion of a grid in front of the detector. Figure 4(b) clearly shows that the electron-induced signal develops a tail to lower energies when grids are inserted, and, as expected, the tail is most pronounced at low transmissions. Furthermore, the tail in the SSD pulse height spectrum appears around 1.2 MeV which is in the energy range where a signal stemming from mass 63 amu would be expected (the mass 63 fragment energy should be lower than $\frac{63}{79}E_{beam}=1.3$ MeV due to the aforementioned energy loss in the dead layer). As no contribution is found around 1.2 MeV in the spectrum taken without a grid, it is concluded that channel (A) is probably dominated by pure detachment.

IV. DISCUSSION

A. Threshold energy

The threshold energy for electron-impact detachment from the four anions is related to their electron binding energy. The incoming electron interacts with the anion on a time scale much shorter than the time scales for molecular vibration and rotation, and hence the molecular geometry essentially remains unchanged during the detachment process. Therefore the threshold energy for detachment must be compared to the *vertical detachment energy* (VDE) rather than the adiabatic electron affinity (EA) (see Ref. [51] for definitions). However, the photoelectron spectra for PO^-

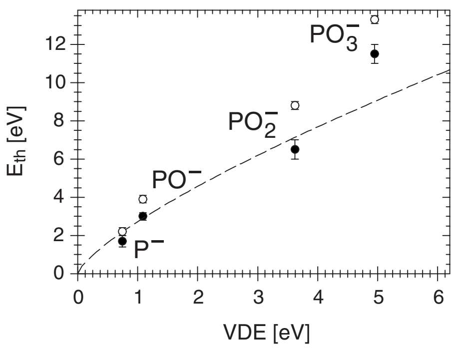

FIG. 5. Measured threshold energy for electron-induced detachment from the PO_n^- anions as a function of their vertical detachment energy (VDE) [52–55]. Filled circles are the onsets as read from the cross section plots, whereas the open circles represent the threshold energies obtained by a fit to the classical model cross section. The dashed line represents the $2^{1/4}(\mathrm{VDE})^{3/4}$ prediction (see text for details).

[52], PO_2^- [53], and PO_3^- [54] show that only PO_2^- exhibits a difference between the EA and VDE, which is found to be 0.2 eV. The threshold energies obtained for the four studied species are shown as a function of their VDE in Fig. 5. Here, both the threshold energy obtained from a direct reading of the cross section onsets as well as the values obtained from the fits of Eq. (2) to the cross section data are plotted. The difference reflects the discrepancies between the measured cross section and the model in the onset region, some of which is due to tunneling.

For atomic anions, the threshold energy E_{th} may be related to the electron binding energy of the anion, E_{b}, and the spatial extent of the binding potential, d, through the equation $E_{\mathrm{th}}=\sqrt{E_{\mathrm{b}}/d}$ (in atomic units) [10,56,57]. In the case of weakly bound atomic anions, the spatial extent of the binding potential scales according to $d\simeq 1/\sqrt{2E_{\mathrm{b}}}$ [58], and combining these two relations gives the following expression for the threshold energy:

$$E_{\mathrm{th}} = \sqrt{\frac{E_{\mathrm{b}}}{d}} \simeq 2^{1/4}E_{\mathrm{b}}^{3/4}. \qquad (7)$$

For molecular anions, the binding energy is replaced by the VDE. The threshold energy predicted by this expression has previously been compared to the experimentally obtained threshold energies for a number of different anions [27], and good agreement was found for the smaller species. This model is also shown in Fig. 5. While giving a fairly good estimate of the threshold energy for the small species, it is underestimating this threshold for the larger molecules, in particular PO_3^-.

A phenomenon that can lead to a higher threshold energy for PO_3^- than expected is the anion polarizability. As the incoming electron approaches the anion, the target electrons respond to its presence by moving toward the opposite side of the binding potential as sketched in Fig. 6. The electric field of the projectile electron changes the potential seen by the target electrons, which results in the appearance of a potential barrier through or over which electrons might escape. However, the increased electron density in the direction opposite the approaching electron increases the barrier height compared to a situation without polarization effects. Thus the incoming electron must carry more energy to cause significant detachment than expected from a model ignoring polarization of the anion. A similar effect has been observed for strong-field ionization of small metal clusters [59]. As compared to a calculation relying on a single-active-electron picture, a dramatic suppression of the ionization was observed in that work. This suppression was attributed to the cluster polarizability, and when including this effect in the calculation, better agreement with the observations was obtained.

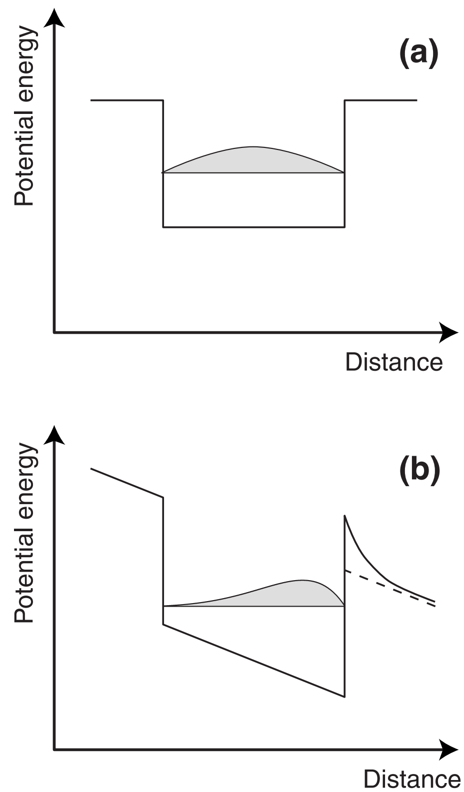

FIG. 6. (a) Sketch of the binding potential of the least bound electron in the undisturbed anion, that is, the effective potential created by the nuclei and the other electrons. (b) Sketch of the total potential experienced by the least bound electron in the presence of the projectile electron. The other electrons also respond to the incoming electron by moving to one side of the potential which leads to a polarization of the anion. Thus the height of the potential barrier that must be penetrated or overcome in order to escape increases (solid line) relative to a model potential which ignores the polarization (dashed line).

To explore the effect of polarization, a comparison of the polarizabilities of the phosphorus oxide anions would be desirable. As an approximation, the polarizability scales with the volume of the molecule [60]. Since the PO_3 anion is the largest of the molecules studied here, it is expected to have the highest polarizability, and consequently it is plausible that any effect stemming from a polarization of the target anion is most pronounced for this anion.

B. Cross section behavior

For P^- and PO^-, the overall shape of the neutralization cross section (neglecting the threshold region) is well described by the classical model [Eq. (2)], which assumes that a detachment reaction occurs with constant probability if the incoming electron comes within a certain distance of the anion. However, for PO_3^-, and partly PO_2^-, the model does not only fail to describe the measured cross section in the near-threshold region but it is furthermore not sufficient to represent the overall shape of the measured cross section, which displays a different curvature than the model. A similar behavior of the cross section was also seen for p-benzoquinone ($C_6H_4O_2^-$) [37], and for some hydroxide-water cluster anions [39]. The discrepancy between the data and the model cross section might be attributed to the geometry of the molecular systems. In the model used above, the reaction zone is chosen to be a sphere with radius $R_{\mathrm{th}}=1/E_{\mathrm{th}}$, which is reasonable for the spherical symmetric atomic anions, but the assumption becomes problematic, for example, planar molecules such as p-benzoquinone and PO_3^-. As already mentioned, the nuclei can essentially be considered fixed in space during the scattering process since the time scales for vibrations and rotations are longer than the collision time scale. The detachment process is thus likely to depend on the orientation of the molecule relative to the impacting electron. This leads to a dependence of the threshold energy on the molecular orientation, and since all orientations are present in the beam, the result is a smearing of the cross section. As a consequence, the model cross section [Eq. (2)] no longer reproduces the observed behavior.

To investigate how an orientational effect as described above might influence the cross section shape, the classical model is extended in the following such that the reaction zone becomes an ellipsoid instead of a sphere. The ellipsoid is characterized by the lengths of three semiaxes, which in the following are collectively denoted by $\boldsymbol{a}$. The orientation of the ellipsoid with respect to a space-fixed frame is described by the three Euler angles, α, β, and γ, collectively referred to as $\boldsymbol{\Omega}$. The reaction probability is now given by

$$P(E,\boldsymbol{\Omega},\boldsymbol{a},\rho,\phi)=\begin{cases} p, & \exists \ \ \theta: D(E,\rho,\phi,\theta) \le R(\boldsymbol{\Omega},\boldsymbol{a},\phi,\theta) \\ 0, & \text{otherwise} \end{cases}, \tag{8}$$

where $D(E,\rho,\phi,\theta)$ is the distance between the incoming electron and the center of the ellipsoid, and $R(\boldsymbol{\Omega},\boldsymbol{a},\phi,\theta)$ describes the surface of the ellipsoid (see Fig. 7). ρ is the impact parameter and θ and ϕ are the polar and azimuthal angles, respectively, of the incoming electron. For a given orientation $\boldsymbol{\Omega}$ of the ellipsoid, the cross section is given by

$$\sigma(E,\boldsymbol{\Omega},\boldsymbol{a})=\int_0^{2\pi}\int_0^{\infty}P(E,\boldsymbol{\Omega},\boldsymbol{a},\rho,\phi)\rho d\rho d\phi. \tag{9}$$

In the ion beam, the ions have random orientations, and the cross section must be averaged over all orientations before it can be compared directly to the data. The orientationally averaged cross section is computed according to

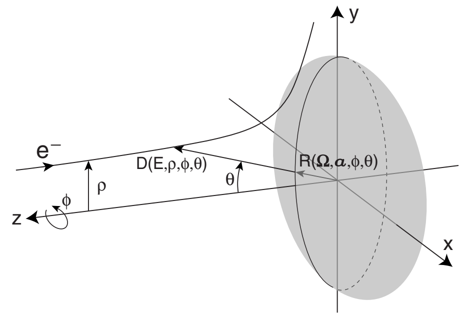

FIG. 7. The scattering of an electron in the field of a central potential. The ellipsoidal reaction zone is indicated by the gray area.

$$\langle\sigma(E,\boldsymbol{a})\rangle=\frac{1}{8\pi^2}\int_0^{2\pi}\int_0^{\pi}\int_0^{2\pi}\sigma(E,\boldsymbol{\Omega},\boldsymbol{a})\sin\beta d\gamma d\beta d\alpha. \tag{10}$$

The reaction probability $P(E,\boldsymbol{\Omega},\boldsymbol{a},\rho,\phi)$ as well as the orientation dependent and the orientational averaged cross sections were calculated numerically for different assumptions on $\boldsymbol{a}$. It should be noted that the *shape* of the cross section only depends on the ratios of the lengths of the three semiaxes, implying that it is determined by only two parameters, while a third parameter determines the overall scale.

In Fig. 2, the model cross section for an elliptical reaction zone is shown (solid curves) together with the experimental data. The relation between the lengths of the three semiaxes was set to 1:0.5:0.5 for PO_2^- and 1:1:0.3 for PO_3^-. These relations were obtained by comparing the measured cross sections to numerically calculated cross sections for different ellipsoids and choosing the ellipsoidal geometry that gave the best agreement between the measured and the model cross section. Remarkably, the obtained ellipsoids are similar to the shapes of the anions: PO_2^- has a bent geometry with an O–P–O bond angle of 119° [53] and PO_3^- has a planar geometry with D_{3h} symmetry [54]. Figure 2(d) shows that the ellipsoidal model gives a significantly better agreement with the measured cross section than the spherical model, implying that an orientational effect could indeed play an important role in the observed energy dependence of the detachment cross section.

C. Dianions

Previous studies of electron-impact detachment of NO_2^- and NO_3^- have shown structures attributed to the formation of short-lived dianions in the detachment cross section of the two anions [25,27]. As the electronic structures of these anions are similar to those of PO_2^- and PO_3^-, it was speculated that dianion states of PO_2 and PO_3 might also be populated in scattering events. However, the detachment cross sections of the phosphorus oxide anions do not show any sign of resonant structures stemming from dianion formation.

For another pair of isoelectronic species, NCO^- and NCS^-, resonant structures have been observed in the detachment cross sections [29]. The energy of the NCO^{2-} resonance was found to be slightly higher than the energy of the lowest-lying NCS^{2-} resonance state owing to the reduced Coulomb repulsion for the latter species [29].

In the case of NO_2^-, two resonance states were observed: one at 7.2 eV above the anion ground state and another at 16.5 eV [25]. Drawing parallels with the findings for NCO^- and NCS^-, two resonance states might also be expected for PO_2^-. However, if existing, the low-energy state of PO_2^{2-} is likely not to be seen in the experiments: presumably, the resonance position will be lower than the 7.2 eV seen for NO_2^- due to the reduced interelectronic Coulomb repulsion in PO_2^-. Since the electron binding energy of PO_2^- is as high as 3.4 eV [53], the emission of two electrons and thus the creation of detectable neutral fragments appears unlikely.

The argument given above does not exclude the possibility of observing a dianion state of PO_2 corresponding to the higher-lying dianion state of NO_2. Furthermore, a dianion state of NO_3 was observed at 18.6 eV above the NO_3^- ground state, and thus for PO_3^{2-} a similar state appears possible. The fact that no such states are observed for neither PO_2^- nor PO_3^- may be ascribed to several effects: (i) the states might not exist, (ii) the dianions might decay by either single-electron autodetachment or Coulomb explosion in which cases no detectable (neutral) fragments emerge from the process, (iii) penetration of the Coulomb barrier at the relevant energies might be suppressed, (iv) the lifetime might be too short to cause a significant structure.

V. CONCLUSION

Electron-impact detachment from PO_n^- (n=0–3) was studied for collision energies in the range from ~0 to ~40 eV. All cross sections exhibit a well-defined onset at an energy significantly larger than the electron binding energy of the target anion. The measured cross sections were compared to a classical model, which provided a good description of the cross section behavior of the smaller ions, when disregarding the region below the classical threshold. For PO_3^-, a nonspherical model was introduced, which improved the agreement with the experimental data.

For the molecular anions, measurements to extract the branching ratios were conducted, and it was found that pure detachment was the dominant reaction channel in all cases. The second most important reaction channel was dissociative detachment with one of the P–O bonds being broken.

In contrast to their isoelectronic species NO_2^- and NO_3^-, neither PO_2^- nor PO_3^- is seen to form transient dianion states when bombarded with electrons.

ACKNOWLEDGMENTS

This work was supported by the Danish Research Foundation through the Aarhus Center for Atomic Physics (ACAP) and the Danish Natural Science Research Council (Grant No. 272-06-0427). We thank the staff at ASTRID for their invaluable assistance during the experiments. Discussions with S. Brøndsted Nielsen are gratefully acknowledged.

[1] G. Tisone and L. M. Branscomb, Phys. Rev. Lett. **17**, 236 (1966).
[2] R. Wildt, Astrophys. J. **89**, 295 (1939).
[3] L. M. Branscomb and S. J. Smith, Phys. Rev. **98**, 1028 (1955).
[4] S. Chandrasekhar, Astrophys. J. **102**, 223 (1945).
[5] B. Peart, D. S. Walton, and K. T. Dolder, J. Phys. B **3**, 1346 (1970).
[6] B. Peart and K. T. Dolder, J. Phys. B **6**, 1497 (1973).
[7] B. Peart, R. A. Forrest, and K. T. Dolder, J. Phys. B **12**, 2735 (1979).
[8] B. Peart, R. Forrest, and K. T. Dolder, J. Phys. B **12**, L115 (1979).
[9] L. H. Andersen, D. Mathur, H. T. Schmidt, and L. Vejby-Christensen, Phys. Rev. Lett. **74**, 892 (1995).
[10] L. Vejby-Christensen, D. Kella, D. Mathur, H. B. Pedersen, H. T. Schmidt, and L. H. Andersen, Phys. Rev. A **53**, 2371 (1996).
[11] T. Tanabe *et al.*, Phys. Rev. A **54**, 4069 (1996).
[12] L. H. Andersen, M. J. Jensen, H. B. Pedersen, L. Vejby-Christensen, and N. Djurić, Phys. Rev. A **58**, 2819 (1998).
[13] K. Andersson *et al.*, Eur. Phys. J. D **13**, 323 (2001).
[14] A. Le Padellec, G. F. Collins, H. Danared, A. Källberg, F. Hellberg, A. Neau, K. Fritioff, D. Hanstorp, and M. Larsson, J. Phys. B **35**, 3669 (2002).
[15] K. Fritioff, J. Sandström, D. Hanstorp, A. Ehlerding, M. Larsson, G. F. Collins, D. J. Pegg, H. Danared, A. Källberg, and A. Le Padellec, Phys. Rev. A **68**, 012712 (2003).
[16] K. Fritioff, J. Sandström, D. Hanstorp, F. Hellberg, A. Ehlerding, M. Larsson, G. F. Collins, D. J. Pegg, H. Danared, and A. Källberg, Eur. Phys. J. D **27**, 23 (2003).
[17] K. Fritioff *et al.*, Phys. Rev. A **69**, 042707 (2004).
[18] L. H. Andersen, P. Hvelplund, D. Kella, P. H. Mokler, H. B. Pedersen, H. T. Schmidt, and L. Vejby-Christensen, J. Phys. B **29**, L643 (1996).
[19] H. B. Pedersen, N. Djurić, M. J. Jensen, D. Kella, C. P. Safvan, L. Vejby-Christensen, and L. H. Andersen, Phys. Rev. Lett. **81**, 5302 (1998).
[20] H. B. Pedersen, N. Djurić, M. J. Jensen, D. Kella, C. P. Safvan, H. T. Schmidt, L. Vejby-Christensen, and L. H. Andersen, Phys. Rev. A **60**, 2882 (1999).
[21] H. B. Pedersen, R. Bilodeau, M. J. Jensen, I. V. Makassiouk, C. P. Safvan, and L. H. Andersen, Phys. Rev. A **63**, 032718 (2001).
[22] A. Le Padellec *et al.*, Phys. Scr. **64**, 467 (2001).
[23] L. H. Andersen, J. Bak, S. Boyé, M. Clausen, M. Hovgaard, M. J. Jensen, A. Lapierre, and K. Seiersen, J. Chem. Phys. **115**, 3566 (2001).
[24] G. F. Collins *et al.*, Phys. Rev. A **72**, 042708 (2005).
[25] L. H. Andersen, R. Bilodeau, M. J. Jensen, S. B. Nielsen, C. P. Safvan, and K. Seiersen, J. Chem. Phys. **114**, 147 (2001).
[26] A. Le Padellec *et al.*, J. Chem. Phys. **115**, 10671 (2001).
[27] K. Seiersen, J. Bak, H. Bluhme, M. J. Jensen, S. B. Nielsen, and L. H. Andersen, Phys. Chem. Chem. Phys. **5**, 4814 (2003).
[28] K. Fritioff *et al.*, J. Phys. B **37**, 2241 (2004).

[29] A. Svendsen, M. O. A. El Ghazaly, and L. H. Andersen, J. Chem. Phys. **123**, 114311 (2005).
[30] L. Lammich *et al.*, Eur. Phys. J. D **41**, 103 (2007).
[31] S. P. Møller, Nucl. Instrum. Methods Phys. Res. A **394**, 281 (1997).
[32] M. Dahan, R. Fishman, O. Heber, M. Rappaport, N. Altstein, D. Zajfman, and W. J. van der Zande, Rev. Sci. Instrum. **69**, 76 (1998).
[33] D. Zajfman, O. Heber, L. Vejby-Christensen, I. Ben-Itzhak, M. Rappaport, R. Fishman, and M. Dahan, Phys. Rev. A **55**, R1577 (1997).
[34] H. Bluhme, M. J. Jensen, S. B. Nielsen, U. V. Pedersen, K. Seiersen, A. Svendsen, and L. H. Andersen, Phys. Rev. A **70**, 020701(R) (2004).
[35] T. Tanabe, K. Noda, M. Saito, E. B. Starikov, and M. Tateno, Phys. Rev. Lett. **93**, 043201 (2004).
[36] A. Diner *et al.*, Phys. Rev. Lett. **93**, 063402 (2004).
[37] M. O. A. El Ghazaly, A. Svendsen, H. Bluhme, S. B. Nielsen, and L. H. Andersen, Chem. Phys. Lett. **405**, 278 (2005).
[38] M. Eritt, A. Diner, Y. Toker, O. Aviv, O. Heber, M. L. Rappaport, and D. Zajfman, Phys. Scr. **73**, C32 (2006).
[39] A. Svendsen, H. Bluhme, K. Seiersen, and L. H. Andersen, J. Chem. Phys. **121**, 4642 (2004).
[40] H. H. Andersen and P. Tykesson, IEEE Trans. Nucl. Sci. **22**, 1632 (1975).
[41] P. Tykesson, H. H. Andersen, and J. Heinemeier, IEEE Trans. Nucl. Sci. **23**, 1104 (1976).
[42] S. P. Møller, in *Conference Record of the 1991 IEEE Particle Accelerator Conference*, edited by L. Lizama (IEEE, New York, 1991), p. 2811.
[43] S. P. Møller, in *Proceedings of the Third European Particle Accelerator Conference*, Berlin, 1992.
[44] L. H. Andersen, J. Bolko, and P. Kvistgaard, Phys. Rev. A **41**, 1293 (1990).
[45] T. J. Morgan, K. H. Berkner, and R. V. Pyle, Phys. Rev. Lett. **26**, 602 (1971).
[46] J. B. A. Mitchell, J. L. Forand, C. T. Ng, D. P. Levac, R. E. Mitchell, P. M. Mul, W. Claeys, A. Sen, and J. W. McGowan, Phys. Rev. Lett. **51**, 885 (1983).
[47] S. Datz, G. Sundström, C. Biedermann, L. Broström, H. Danared, S. Mannervik, J. R. Mowat, and M. Larsson, Phys. Rev. Lett. **74**, 896 (1995).
[48] L. H. Andersen, O. Heber, D. Kella, H. B. Pedersen, L. Vejby-Christensen, and D. Zajfman, Phys. Rev. Lett. **77**, 4891 (1996b).
[49] *NIST Chemistry WebBook*, URL: http://webbook.nist.gov/chemistry/
[50] J. D. Jackson, *Classical Electrodynamics*, 3rd ed. (Wiley, New York, 1999), Chap. 13.
[51] J. C. Rienstra-Kiracofe, G. S. Tschumper, H. F. Schaefer, S. Nandi, and G. B. Ellison, Chem. Rev. **102**, 231 (2002).
[52] P. F. Zittel and W. C. Lineberger, J. Chem. Phys. **65**, 1236 (1976).
[53] C. Xu, E. de Beer, and D. M. Neumark, J. Chem. Phys. **104**, 2749 (1996).
[54] X.-B. Wang and L.-S. Wang, Chem. Phys. Lett. **313**, 179 (1999).
[55] D. Feldmann, Z. Phys. A **277**, 19 (1976).
[56] E. A. Solov'ev, Sov. Phys. JETP **45**, 1089 (1977).
[57] V. N. Ostrovsky and K. Taulbjerg, J. Phys. B **29**, 2573 (1996).
[58] B. M. Smirnov, *Negative Ions* (McGraw-Hill, Inc., New York, 1982).
[59] M. Smits, C. A. de Lange, A. Stolow, and D. M. Rayner, Phys. Rev. Lett. **93**, 203402 (2004).
[60] P. Atkins and R. Friedman, *Molecular Quantum Mechanics* (Oxford University Press, New York, 2005).